Desalination and Water Treatment
www.deswater.com
doi: 10.1080/19443994.2013.877855

54 (2015) 540–546
April

Taylor & Francis
Taylor & Francis Group

Cu_2O immobilized on reduced graphene oxide for the photocatalytic treatment of red water produced from the manufacture of TNT

Bo Shen, Yihe Zhang*, Qi An, Li Yu, Jiwu Shang

National Laboratory of Mineral Materials, School of Materials Science and Technology, China University of Geosciences, Beijing 10083, China
Tel./Fax: +86 10 82323433; email: zyh@cugb.edu.cn

Received 31 October 2013; Accepted 9 December 2013

ABSTRACT

In this paper, we report on the synthesis of nanocomposite catalysts composed of cuprous oxide (Cu_2O) and reduced graphene oxide (rGO) formed at room temperature. The nanocomposites were characterized by X-ray diffraction, transmission electron microscopic analysis, ultraviolet-visible diffuse reflection absorptive spectroscopy, etc. The results show that the cuprous oxide particles can be immobilized on the surface of rGO and that the rGO improves the optical properties of Cu_2O thereby enhancing the utilization of visible light. Compared with Cu_2O under similar synthesis condition, the Cu_2O/rGO composites demonstrate improved photodegradative activity of red water. This study verifies the viability of the use of Cu2O/rGO composites in the treatment of red water.

Keywords: Cuprous oxide; Reduced graphene oxide; Composites; Red water; Photocatalysis

1. Introduction

Since it was first synthesized by Joseph Wilbrand in 1863, trinitrotoluene (TNT; 2,4,6-trinitrotoluene) has been widely used as an explosive in many applications because of its superior properties such as the low manufacturing cost, high explosive power, and low melting point [1]. Large-scale production of TNT results in the generation of large quantities of wastewater which has historically been an environmental hazard due to the toxic and mutagenic effects of TNT [2,3]. Red water is the wastewater produced when crude TNT is purified using sodium sulfite. This product is dark red and contains hazardous materials such as trinitrotoluene, nitrotoluene, dissolved dinitrotoluene sulfonates (mainly 4-dinitrotoluene-3-sulfonate and 2,4-dinitrotoluene-5-sulfonate), dinitrotoluene, and other materials [4]. Currently, adsorption is the most widely used method to treat red water [5,6]. Other treatment methods include incineration, degradation utilizing microorganisms [7], advanced oxidation using UV, hydrogen peroxide/ozone [8] and supercritical water treatment [9]. However, it has been found that the decomposition products of the oxidation processes may be even more hazardous than the original pollutant. Photocatalytic technology has attracted much attention due to its ability to completely remove organic pollutants in process effluent. Unlike conventional biodegradation or adsorption methods, photocatalytic technology offers a powerful way to treat bio-resistant organic contaminants by converting them into smaller molecules such as CO_2 [10].

*Corresponding author.

1944-3994/1944-3986 © 2013 Balaban Desalination Publications. All rights reserved.

As a versatile semiconductor, Cu_2O has attracted increasing attention by researchers, because of its promising applications in hydrogen production [11], lithium ion batteries [12], solar energy [13], biosensors [14], magnetic storage devices [15], catalysis [16], and gas sensor [17]. Due to the narrow direct band gap of this material (2.0–2.2 eV) and its suitable energy level position [18], Cu_2O can be activated by visible light irradiation which constitutes about 50% of sunlight. This feature makes Cu_2O more desirable for visible light applications than conventional photocatalysts such as TiO_2 and ZnO. Additionally, compared with other narrow band gap semiconductors such as metal sulfides, Cu_2O exhibits low toxicity and low cost making it environmentally friendly and attractive for large-scale applications. Because of these properties, there has been considerable work in recent years examining the photocatalytic treatment of organic pollutants using cuprous oxide as the catalyst. To promote the photocatalytic performance of this material, porous matter, such as silicon oxide [19], aluminum oxide [20], and activated carbon [21], has been used as high-surface-area supports for cuprous oxide. In our previous study [22], we chose to immobilize Cu_2O on sepiolite and reported that the photocatalytic activity of this composite for the degradation of red water was better than unsupported Cu_2O.

Graphene is a novel two-dimensional material that has attracted much attention since its experimental discovery in 2004, because of its excellent physical and chemical properties [23,24]. Graphene and graphene oxide (GO) have potential application as a catalyst support in the field of catalysis. Compared to conventional porous carbon materials, graphene offers a higher surface area to support metal nanoparticles, which could lead to higher catalyst utility. For example, cuprous oxide/graphene nanocomposites had been synthesized as an efficient electrocatalyst for oxygen reduction reaction [25] and its application in an electrochemical sensor for dopamine had been reported [26]. In this study, we immobilized Cu_2O onto rGO, and used the composite material as photocatalyst for the decomposition of red water. The Cu_2O–rGO composite materials were characterized in detail and the photocatalytic activity for the treatment of the red water was discussed thoroughly in relation to the morphologies and the preparative conditions of the catalyst. The activity of the photocatalyst prepared under optimized conditions was significantly improved over the two singular components in the composite, (i.e. Cu_2O or rGO) when they were used individually. Our experimental results suggest that rGO plays an important role in enhancing the photocatalytic activity of Cu_2O and the Cu_2O/rGO composite appears to be an effective photocatalyst for the treatment of the red water.

2. Experimental

2.1. Preparation of GO

Natural graphite powder (particle size 60 μm) was oxidized using the modified Hummer's method to produce GO [27]. In this method, graphite (5 g) and concentrated H_2SO_4 (120 mL) were added to a 1,000 mL erlenmeyer flask with stirring in an ice bath. $KMnO_4$ (15 g) was added slowly in portions to keep the reaction temperature below 5˚C and the mixture was stirred for 60 min in an ice bath. Following this, the ice bath was removed and the dark green solution was continuously stirred at 35˚C for 60 min. Subsequently, 200 mL of DI water was added slowly to the reaction mixture and the erlenmeyer flask was warmed in an oil bath to 98˚C and held at this temperature for another 60 min. Finally, 360 mL of deionized water and 10 mL of 80% H_2O_2 were added to the reaction mixture to stop the reaction. The precipitate was centrifuged and washed repeatedly with 5% HCl and ethanol and then vacuum dried by lyophilization.

2.2. Preparation of Cu_2O/rGO

Cu_2O nanoparticles were deposited on graphene by chemical reduction of $CuSO_4$ in the presence of GO. Various amounts of rGO were added to the Cu_2O synthesis system to produce Cu_2O/rGO composites with various Cu_2O loadings. The quantities of reduced GO (0, 100, 200, 300, 400, or 500 mg) were ultrasonically dissolved in 150 mL of water. Then, 10 mmol $CuSO_4$ was dissolved in 50 mL of water and added into each of the rGO solutions under ultrasound conditions to form a uniform dispersion. Following this, 20 mmol NaOH was dissolved in each of the above solutions. The resultant mixtures were stirred for 60 min to produce a blue flocky precipitate. Next, 10 mmol L-ascorbic acid was then added into each separate solution and each was stirred for another 60 min, this produced a color change in the precipitate from blue to light yellow. The resulting precipitates were collected and washed repeatedly with ethanol and then lyophilized. This procedure produced six samples which were denoted as A1–A6. The entire preparation process is shown in Fig. 1.

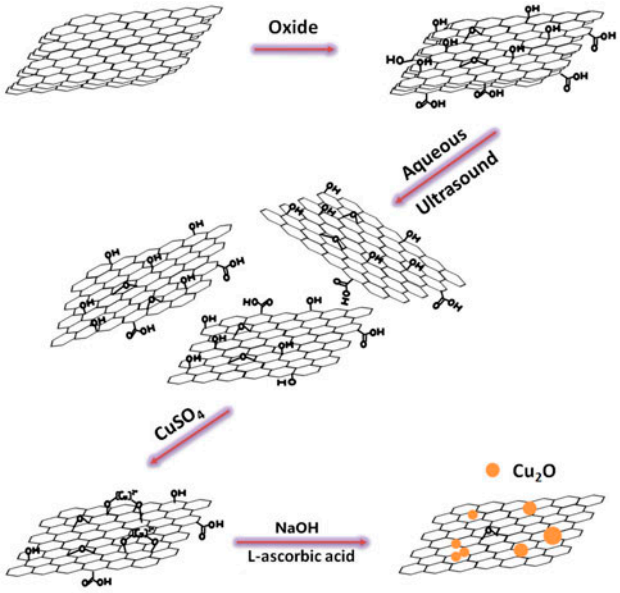


Fig. 1. Schematic presentation for the preparation procedure of Cu_2O/rGO.

2.3. Characterization and properties

The crystal structure of the synthesized particles was determined using X-ray diffraction (XRD, Rigaku D/Max-Ra). The samples were scanned at 8°/min from 5° to 80° using Cu-Kα radiation ($\lambda = 0.154056$ nm) at a filament voltage of 40 kV and current of 100 mA. The morphologies and compositions of the resulting products were studied by transmission electron microscopy (TEM) and Fourier transformation infrared spectroscopy (FT-IR). TEM images were obtained on a JEM2010 microscope at 200 kV. The samples were prepared by drying a droplet of each suspension (5×10^{-4} g/mL) on 400-mesh carbon-coated copper grids. The FT-IR spectra of the samples were acquired on a Perkin–Elmer Spectrum 100 FT-IR spectrophotometer in the range of 4,000–400 cm^{-1}. Test samples were prepared using potassium bromide to form a test pellet. The ultraviolet–visible diffuse reflection absorptive spectra (UV–vis/DRS) were obtained at room temperature on a Lambda-900 UV/vis/NIR spectrometer (Perkin–Elmer, USA) equipped with an integration sphere.

2.4. Photocatalysis measurement

The red water produced from TNT manufacturing was obtained from Dongfang Chemical Corporation (Hubei Province, China). The red water was diluted 200 times with deionized water, because the original red water is too dense to be treated efficiently photocatalytically. The chemical oxygen demand (COD) of the diluted red water used in this study was found to be 1,025 mg/L. To achieve adsorption equilibrium, 20 mg of each Cu_2O/rGO sample (A1–A6) was ultrasonically dispersed in 100 mL of diluted red water which was loaded into a water-cooled double-walled-beaker and the mixture was stirred in the dark for 30 min. The photocatalytic experiments were carried out in a reactor equipped with magnetic stirring and a mercury tungsten blended lamp (500 W) positioned about 12.5 cm above the solution surface. At an interval of 60 min from the start of the photoreaction, 10 mL of the suspension was sampled and filtrated. The clarified filtrates were analyzed by a COD rapid detector (5B-6, Lian-Hua Tech. Co., China) with a precision of ± 5% to determine the photocatalytic efficiency of the samples.

3. Results and discussion

Fig. 2 shows the FTIR spectra of the GO, Cu_2O, and Cu_2O/rGO composites. The results indicate that Cu_2O nanoparticles were successfully immobilized onto rGO. Reduced GO exhibits abundant oxygen containing groups. The strong band at 3,410 cm^{-1} results from the stretching vibration of the hydroxyl (–OH) group. The band at 1,730 cm^{-1} is caused by the C=O vibration of –COOH. The peak at 1,620 cm^{-1} may result from skeletal vibrations of the graphitic backbone. The band at 1,387 cm^{-1} can be assigned to the tertiary C–OH group stretching vibration, and the peak at 1,060 cm^{-1} is attributed to C–O stretching vibrations. These characteristic vibrational bands are

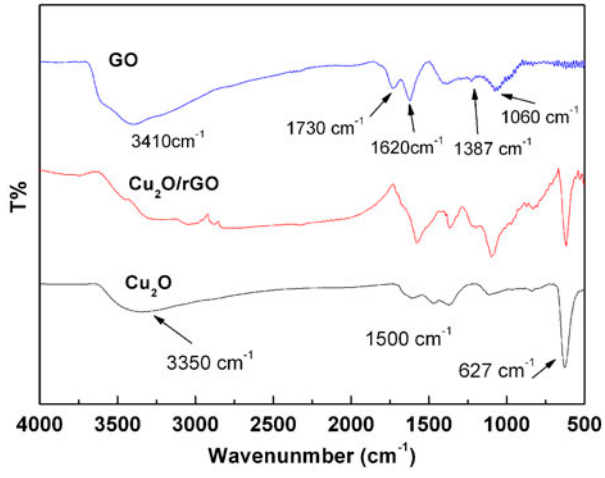


Fig. 2. FTIR of GO, Cu_2O, and Cu_2O/rGO.

indicative that the graphene contains epoxide groups, hydroxyls, and carboxyls. With respect to the Cu_2O, the peak at 627 cm^{-1} is due to Cu–O vibration, the band located at 3,350 cm^{-1} and the peaks near 1,500 cm^{-1} are caused by the stretching and bending vibrations of hydroxyl groups of the adsorbed water.

Referring to the spectra of the Cu_2O/rGO composites, the Cu–O vibration of Cu_2O shifts slightly to 618 cm^{-1}, which might be due to the interaction between Cu_2O and graphene, which perturbs the Cu–O bonds. The characteristic absorbance bands of GO disappear, while the C–O stretching vibrations are still present at 1,060 cm^{-1}. These results indicate that L-ascorbic acid can reduce $Cu(OH)_2$ and partially reduce GO to produce Cu_2O/rGO composites.

XRD spectra confirm the conclusions derived from FTIR spectra. Fig. 3 shows the XRD patterns of GO and the as-prepared Cu_2O/rGO composites. The GO provided a peak centered at $2\theta = 9.12^\circ$, corresponding to the interlayer spacing of the GO of 0.97 nm, which is dramatically larger than the layered spacing of graphite (0.34 nm, $2\theta = 26^\circ$). This means that the space between the graphite sheets has been expanded by oxygen containing groups. In Fig. 3, according to the JCPDS card No.05-0667, the diffraction peaks of Cu_2O (A1) are observed at 2θ values of 29.5°, 36.5°, 42.3°, 61.6°, and 73.5° corresponding to the crystal planes of (110), (111), (200), (220), and (311) of crystalline cuprous oxide. No peaks belonging to Cu or $Cu(OH)_2$ are detected, indicating the efficient conversion of Cu $(OH)_2$ to Cu_2O by the L-ascorbic acid reduction. With respect to the Cu_2O/GO composites (A2–A6), the peaks of Cu_2O are present in XRD patterns, but no characteristic peaks corresponding to GO or graphite

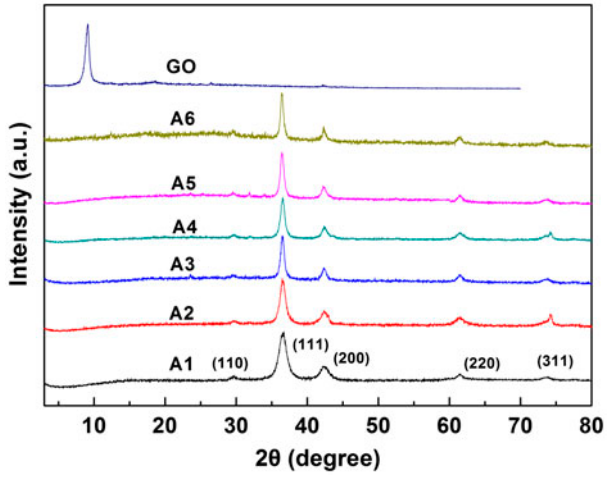


Fig. 3. XRD pattern of Cu_2O (A1), Cu_2O/rGO composites (A2–A6: GO = 50, 100, 150, 200, and 250 mg), and GO.

are observed indicating that the immobilization of Cu_2O onto graphene sheets disturbs the ordered structure of GO or graphite.

The morphologies of Cu_2O/rGO composites were observed using TEM. Fig. 4 shows TEM images of Cu_2O (A1) and Cu_2O/rGO composites (A2–A6) are synthesized with increasing amount of GO. It can be clearly seen in Fig. 4 A1 that the Cu_2O spheres (A1) reduced by L-ascorbic without the presence of GO are comprised of smaller Cu_2O particles and the diameter of the spheres is about 100 nm. As for A2, Cu_2O nanoparticles with diameters of about 40 nm form a dense cover on the rGO sheet and some of these particles have subsequently aggregated. In A3, in addition to the 40 nm Cu_2O nanoparticles as in A2, smaller 5 nm Cu_2O nanoparticles are also seen on the rGO sheet. In sample A4, the smaller Cu_2O nanoparticles are densely scattered over the rGO sheet with larger Cu_2O nanoparticles aggregated, the wrinkles of rGO sheet can be clearly observed. In A5 and A6, with a further increase in the quantity of rGO added to the Cu_2O solution, only a few aggregates appear on the rGO sheet which is composed of large Cu_2O nanoparticles. These TEM images revealed that the oxygen containing groups on GO sheet can act as anchoring sites for the deposition of Cu_2O nanoparticles. There are no Cu_2O nanoparticles scattered outside of the rGO sheet, indicating a strong interaction between rGO support and Cu_2O nanoparticles. Appropriate amounts of GO in the reaction favors the homogeneous scattering of Cu_2O nanoparticles on rGO sheet with smaller particle size and good dispersion. This result suggests a further improvement in the photocatalytic activity of Cu_2O/rGO composites.

The UV–vis DRS of Cu_2O and Cu_2O/rGO (A4) are displayed in Fig. 5(a). The absorption edge of Cu_2O exists at around 630 nm. The absorption edge of the Cu_2O/rGO appears to be somewhat blue shifted. However, the absorbance of Cu_2O and Cu_2O/rGO is similar in the ultraviolet range, while Cu_2O/rGO exhibits higher absorbance in the visible range light than the pure Cu_2O. Since rGO is a black support, it has a large absorbance in visible light range. Consequently, the absorbance of composite in the visible light range can be attributed primarily to the rGO.

To further study the optical properties of the composites, we estimated the band gap energy. The direct band gap is one of the most desirable properties of photocatalyst, because this type of material can absorb photo energy more efficiently than a material with an indirect band gap [28]. Since Cu_2O is a direct gap semiconductor, the relationship between the absorption coefficient (α) and photon energy ($h\nu$) can be expressed as [29]:

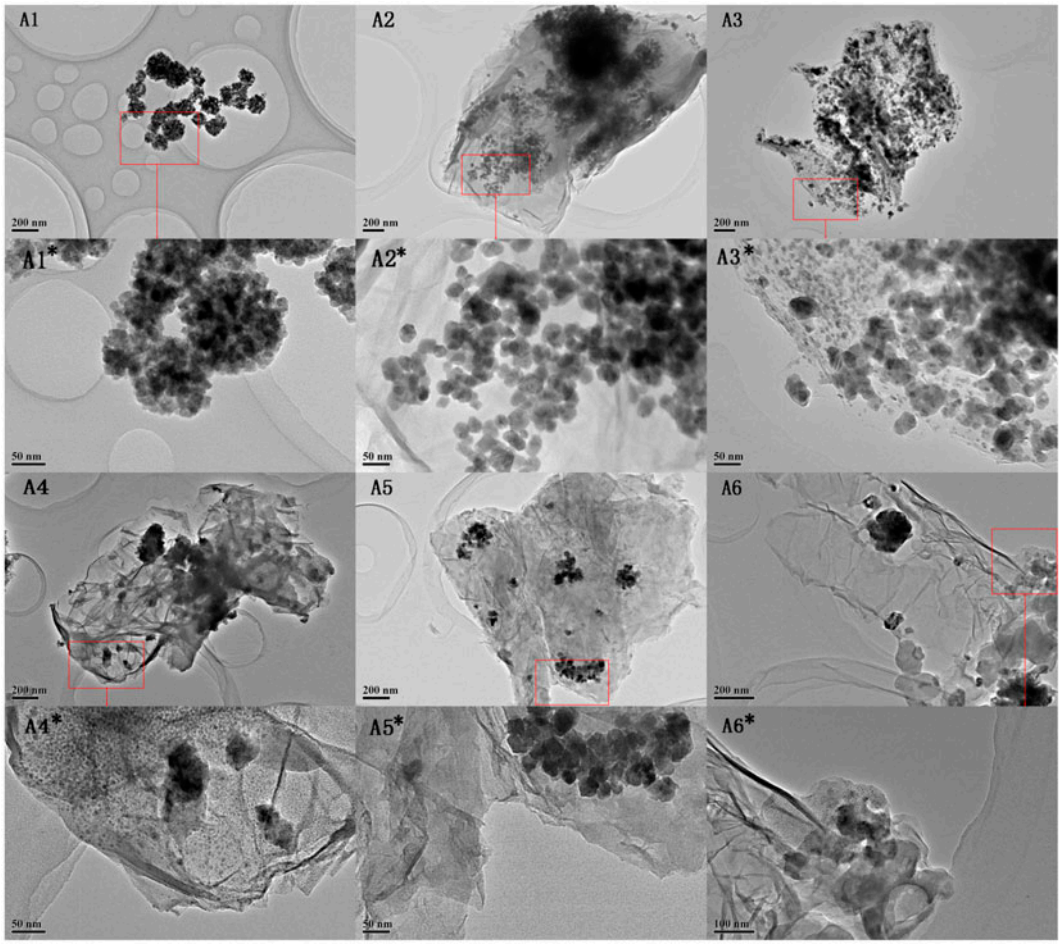


Fig. 4. TEM of pure Cu_2O (A1) and Cu_2O/rGO composites (A2–A6: GO = 50, 100, 150, 200, and 250 mg). AX*(X = 1,2 … 6) is the enlarged image of the corresponding area in AX, denoted with red rectangular.

$$\alpha hv = C(hv - Eg)^{1/2} \quad (1)$$

where C is a constant that is independant of photon energy, Eg is the band gap energy, and α is the absorbance coefficient. The band gap can be estimated from the intercepts of the tangents to the $(\alpha hv)^2$ vs. photon energy (hv) plots. Fig. 5(b) depicts the plots of $(\alpha hv)^2$ vs. (hv) for pure Cu_2O and Cu_2O/rGO. The direct band gaps of pure Cu_2O and Cu_2O/rGO are estimated to be 2.23 and 2.07 eV, respectively. There is a slight red shift in the direct band gap occurs when cuprous oxide is immobilized on rGO. The electrical properties of the rGO improve the surface optical property of the Cu_2O nanoparticles, which lowers the activation energy of Cu_2O crystals and enhances their sensitivity to light.

The photocatalytic activity of Cu_2O and Cu_2O/rGO composites (corresponding to A1–A6 in Fig. 3) was assessed by monitoring the degradation of TNT in the processed red water when exposed to visible light. Red water from TNT manufacturing is a mixture of complex constituents and every constituent has a characteristic absorption wavelength. Therefore, it is very difficult to determine the photocatalytic degradation rate using absorption spectrophotometry. In this study, we determined the degradation of red water by measuring the COD of the red water and the relative removal rates of COD were calculated by the following equation:

$$\text{Relative removal of COD } (\%) = (\text{CODo} - \text{CODe})/\text{CODo} \times 100\%$$

Here, CODo and CODe are the original and final COD values of the TNT red water, respectively. In this equation, the relative removal of COD serves as an indicator of the photolysis rate of red water. Fig. 6 shows that the direct photolysis rate of red water is 1.54%,

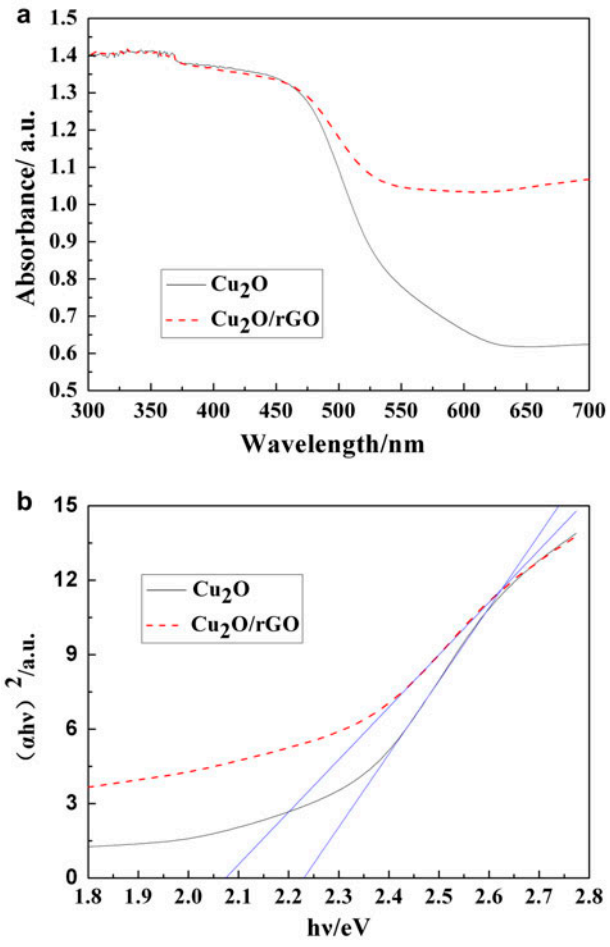


Fig. 5. (a) UV–vis DRS of pure Cu_2O and Cu_2O/rGO(for the sample A4); (b) plots of $(\alpha hv)^2$ vs. hv of Cu_2O and Cu_2O/rGO (for the sample A4).

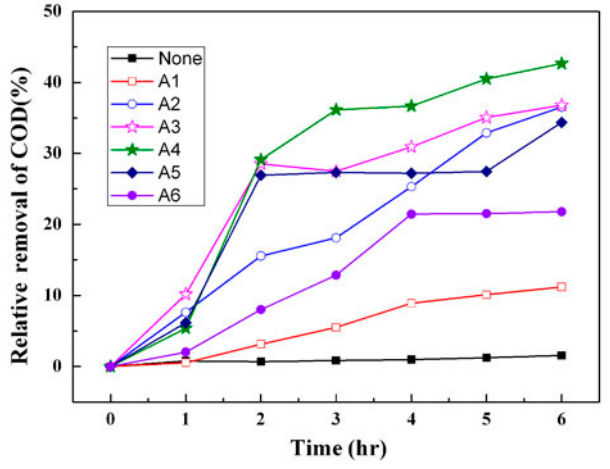


Fig. 6. Photodegradation of red water catalyzed by Cu_2O (A1) and Cu_2O/rGO composite (A2–A6: A2–A6: GO = 50, 100, 150, 200, and 250 mg) under visible light.

when the solution was irradiated using visible light for 6 h without any photocatalysts. This is the baseline result and shows that that direct photolysis of red water does not greatly degrade the dissolved TNT.

The photocatalytic activity of Cu_2O in Sample A1 appears to be low as only 11.2% of organics in red water were degraded. The photodegradation activities of Cu_2O/rGO composites (A2–A6) are significantly enhanced compared with pure Cu_2O, and the largest photolysis rate of red water was 42.6%. The improvement in photocatalytic activity of Cu_2O/rGO composites is due to the efficient retardation in the recombination process of photo-generated electron/hole pairs. Graphene has excellent electrical properties; the work function has been calculated to be 4.42 eV [30]. In addition, the conduction band position of Cu_2O is –3 eV (using vacuum level as a reference) [31]. This means that graphene can accept conduction band electrons from Cu_2O so that the conduction band electrons of Cu_2O can be transferred to graphene, instead of recombining with valence band electron holes in the Cu_2O. This increases the photocatalytic activity of the supported Cu_2O.

On the other hand, the appropriate amount of rGO in the composite catalyst is crucial in determining the photocatalytic activity of the material. Sample A4 exhibits the maximized photocatalytic activity, where about 42.6% of organics in red water was decomposed in 6 h, which is dramatically higher than Cu_2O catalyst. This result combined with the TEM image of A4 implies that an optimum quantity of rGO can favor the homogeneous scattering of the Cu_2O nanoparticles. The appropriate size and dispersion of Cu_2O nanoparticles on rGO sheets appear to have led to more efficient interactions between rGO and Cu_2O resulting in a retardation of the recombination of the electron/hole pairs. This appears to enhance the photocatalytic activity. In the case of samples A2 and A3, Cu_2O nanoparticles were larger or they aggregated on the rGO sheets. This appeared to decrease the efficiency of its interaction between the Cu_2O and the rGO, which hindered the overall activity of combined photocatalyst. In samples A5 and A6, the amount of Cu_2O in composites appeared to be insufficient which resulted in a decrease in the transferred electrons from excitation state of Cu_2O apparently reducing the photocatalytic activity of these two composite catalysts.

4. Conclusions

In summary, Cu_2O/rGO composites with improved photocatalytic activity for the decomposition of the red water were successfully synthesized. TEM images reveal that Cu_2O nanoparticles were

immobilized on rGO sheets. UV–vis DRS analysis revealed that composites improved the optical properties of cuprous oxide and red shifts the band gap, thereby improving the utilization of visible light. The results of the photocatalytic treatment of red water using these experimental materials suggest that the Cu_2O/rGO composites offer excellent photocatalytic performance for degrading the contaminants in the red water that result from the manufacture of TNT.

References

[1] C. Park, T.H. Kim, S. Kim, S.W. Kim, Optimization for biodegradation of 2,4,6-trinitrotoluene (TNT), J. Biosci. Bioeng. 95 (2003) 567–571.

[2] D.J. Luning Prak, Solubilization of nitrotoluenes in micellar nonionic surfactant solutions, Chemosphere 68 (2007) 1961–1967.

[3] N.R. Adrian, C.M. Arnett, Anaerobic biotransformation of explosives in aquifer slurries amended with ethanol and propylene glycol, Chemosphere 66 (2007) 1849–1856.

[4] Q.L. Zhao, Z.F. Ye, M.H. Zhang, Treatment of 2,4, 6-trinitrotoluene (TNT) red water by vacuum distillation, Chemosphere 80 (2010) 947–950.

[5] C. Rajagopal, J.C. Kapoor, Development of adsorptive removal process for treatment of explosives contaminated wastewater using activated carbon, J. Hazard. Mater. 87 (2001) 73–98.

[6] J.W. Lee, T.H. Yang, W.G. Shim, T.O. Kwon, I.S. Moon, Equilibria and dynamics of liquid-phase trinitrotoluene adsorption on granular activated carbon: Effect of temperature and pH, J. Hazard. Mater. 141 (2007) 185–192.

[7] W.Y. Tang, S.F. Zhou, L.J. Wang, Q.T. Peng, Mechanism study of biodegradation TNT wastewater, in: Proc. 3rd Int. Symposium on Pyrotechnics and Explosives, Beijing, 1995, pp. 267–270.

[8] Y.G. Wu, J. Jiao, D.W. Zhao, Advanced oxidation processes for treatment of wastewater contaminated by explosives, J. Energetic Mater. 11 (2003) 166–169.

[9] S.J. Chang, Y.C. Liu, Degradation mechanism of 2,4,6-trinitrotoluene in supercritical water oxidation, J. Environ. Sci. 19 (2007) 1430–1435.

[10] M.R. Hoffmann, S.T. Martin, W. Choi, D.W. Bahnemann, Environmental applications of semiconductor photocatalysis, Chem. Rev. 95 (1995) 69–96.

[11] L.F. Gou, C.J. Murphy, Solution-phase synthesis of Cu_2O nanocubes, Nano Lett. 3 (2003) 231–234.

[12] P. Poizot, S. Laruelle, S. Grugeon, L. Dupont, J.M. Taracon, Nano-sized transition-metal oxides as negative-electrode materials for lithium-ion batteries, Nature 407 (2000) 496–499.

[13] R.N. Briskman, A study of electrodeposited cuprous-oxide photovoltaic cells, Sol. Energy Mater. Sol. Cells 27 (1992) 361–368.

[14] H.T. Zhu, J.X. Wang, G.Y. Xu, Fast synthesis of Cu_2O hollow microspheres and their application in DNA biosensor of hepatitis B virus, Cryst. Growth Des. 9 (2009) 633–638.

[15] X.D. Li, H.S. Gao, C.J. Murphy, L.F. Gou, Nanoindentation of Cu_2O nanocubes, Nano Lett. 4 (2004) 1903–1907.

[16] Z.C. Orel, A. Anžlovar, G. Dražić, M. Žigon, Cuprous oxide nanowires prepared by an additive-free polyol process, Cryst. Growth Des. 7 (2007) 453–458.

[17] J.T. Zhang, J.F. Liu, Q. Peng, X. Wang, Y.D. Li, Nearly monodisperse Cu_2O and CuO nanospheres: Preparation and applications for sensitive gas sensors, Chem. Mater. 18 (2006) 867–871.

[18] L. Huang, F. Peng, H. Yu, H.J. Wang, Preparation of cuprous oxides with different sizes and their behaviors of adsorption, visible-light driven photocatalysis and photocorrosion, Solid State Sci. 11 (2009) 129–138.

[19] W. Chang, Y. Shen, A. Xie, W. Tong, Preparation of Al_2O_3-supported nano-Cu_2O catalysts for the oxidative treatment of industrial wastewater, Russ. J. Phys. Chem. A. 83 (2009) 2308–2312.

[20] X. Zhang, D. Zhang, X. Ni, H. Zheng, Synthesis and optical properties of Cu_2O/SiO_2 composite films via gamma-irradiation route, Mater. Lett. 61 (2007) 248–250.

[21] Z. Li, C.M. Wen, H.Y. Zheng, K.C. Xie, Effects of the active carbon surface properties on the structure and catalytic activity of Cu_2O/AC catalyst chemical, Chem. J. Chin. U. 31 (2010) 145–152.

[22] Q. Zhu, Y. Zhang, F. Lv, P.K. Chu, Z. Ye, F. Zhou, Cuprous oxide created on sepiolite: preparation, characterization, and photocatalytic activity in treatment of red water from 2,4,6-trinitrotoluene manufacturing, J. Hazard. Mater. 217-218 (2012) 11–18.

[23] K.S. Novoselov, A.K. Geim, S.V. Morozov, D. Jiang, Y. Zhang, S.V. Dubonos, I.V. Grigorieva, A.A. Firsov, Electric field effect in atomically thin carbon films, Science 306 (2004) 666–669.

[24] C. Lee, X.D. Wei, J.W. Kysar, J. Hone, Measurement of the elastic properties and intrinsic strength of monolayer graphene, Science 321 (2008) 385–388.

[25] X.Y. Yan, X.L. Tong, Y.F. Zhang, X.D. Han, Y.Y. Wang, G.Q. Jin, Y. Qin, X.Y. Guo, Cuprous oxide nanoparticles dispersed on reduced graphene oxide as an efficient electrocatalyst for oxygen reduction reaction, Chem. Commun. 48 (2012) 1892–1894.

[26] F.Y. Zhang, Y.J. Li, Y. Gu, Z.H. Wang, C.M. Wang, One-pot solvothermal synthesis of a Cu_2O/Graphene nanocomposite and its application in an electrochemical sensor for dopamine, Microchimica Acta. 173 (2011) 103–109.

[27] C. Nethravathi, M. Rajamathi, Chemically modified graphene sheets produced by the solvothermal reduction of colloidal dispersions of graphite oxide, Carbon. 46 (2008) 1994–1998.

[28] R. Shi, J. Lin, Y.J. Wang, J. Xu, Y.F. Zhu, Visible-light photocatalytic degradation of $BiTaO_4$ photocatalyst and mechanism of photocorrosion suppression, J. Phys. Chem. C 114 (2010) 6472–6477.

[29] A.M. Salem, M.S. Selim, Structure and optical properties of chemically deposited Sb_2S_3 thin films, J. Phys. D: Appl. Phys. 34 (2001) 12–17.

[30] R. Czerw, B. Foley, D. Tekleab, A. Rubio, P.M. Ajayan, D.L. Carroll, Substrate-interface interactions between carbon nanotubes and the supporting substrate, Phys. Rev. B 66 (2002) 033408.

[31] L.L. Wu, L.K. Tsui, N. Swami, G. Zangari, Photoelectrochemical stability of electrodeposited Cu_2O films, J. Phys. Chem. C 114 (2010) 11551–11556.